INTERNATIONAL JOURNAL FOR NUMERICAL METHODS IN FLUIDS
Int. J. Numer. Meth. Fluids 2003; **42**:361–382 (DOI: 10.1002/fld.517)

Numerical investigation from rarefied flow to continuum by solving the Boltzmann model equation

Zhi-Hui Li[1,2,*,†] and Han-Xin Zhang[2]

[1] *Department of Engineering Mechanics, Tsinghua University, Beijing 100084, People's Republic of China*
[2] *China Aerodynamics Research and Development Center, P.O. Box 211, Mianyang 621000, People's Republic of China*

SUMMARY

Based on the Bhatnagar–Gross–Krook (BGK) Boltzmann model equation, the unified simplified velocity distribution function equation adapted to various flow regimes can be presented. The reduced velocity distribution functions and the discrete velocity ordinate method are developed and applied to remove the velocity space dependency of the distribution function, and then the distribution function equations will be cast into hyperbolic conservation laws form with non-linear source terms. Based on the unsteady time-splitting technique and the non-oscillatory, containing no free parameters, and dissipative (NND) finite-difference method, the gas kinetic finite-difference second-order scheme is constructed for the computation of the discrete velocity distribution functions. The discrete velocity numerical quadrature methods are developed to evaluate the macroscopic flow parameters at each point in the physical space. As a result, a unified simplified gas kinetic algorithm for the gas dynamical problems from various flow regimes is developed. To test the reliability of the present numerical method, the one-dimensional shock-tube problems and the flows past two-dimensional circular cylinder with various Knudsen numbers are simulated. The computations of the related flows indicate that both high resolution of the flow fields and good qualitative agreement with the theoretical, DSMC and experimental results can be obtained.

KEY WORDS: Boltzmann model equation; gas kinetic theory; discrete velocity ordinate method; NND finite-difference scheme; rarefied gas flow; continuum flow

1. INTRODUCTION

In order to study the aerodynamics from various flow regimes, the traditional way is to deal with them with different methods, such as the Monte-Carlo method for rarefied flow and the

* Correspondence to: Li Zhihui, Department of Enginerring Mechanics, Tsinghua University, 100084 Beijing, China.
† E-mail: zhli0097@x263.net

Contract/grant sponsor: National Nature Science Foundation of China; contract/grant number: 19972008
Contract/grant sponsor: National Nature Science Foundation of China; contract/grant number: 10072077

Received 17 April 2002
Revised 16 October 2002

Navier–Stokes (N–S) equations for the continuum flow. Both the methods are totally different, and the computational results are difficult to be linked up smoothly with altitude. In this study, it is to be considered whether a unified numerical algorithm to predict the gas flows over the complete spectrum of flow regimes can be found.

The Boltzmann equation [1] can describe molecular transport phenomena of various flow regimes and act as the main foundation for the study of gas dynamics. However, it is very difficult to accurately solve the Boltzmann equation describing complex flows. On the other way round, based on the mass, momentum and energy conservation laws, kinds of kinetic model equations [2–4] resembling to the original Boltzmann equation concerning the various order of moments have been put forward with applying the basic characteristics of molecular movement and collision approaching to equilibrium. Based on the zeroth, first and second-order approximation of the Maxwellian distribution, the Euler, N–S and Burnett equation describing the macroscopic gas dynamics can be, respectively, deduced by applying the Chapmann–Enskog procedure [1, 5] to the Boltzmann equation or the simple Bhatnagar–Gross–Krook (BGK) model equation [2]. Formerly, it was considered that the BGK equation only describes the flows in the equilibrium or near equilibrium state [1, 6]. Nowadays, it is suggested from References [4, 7–9] that the equation can also qualitatively characterize the complex gas flows from various flow regimes by revising its collision relaxation parameter and local equilibrium distribution function. Thus, as a qualitative method, instead of solving the full Boltzmann equation one solves the modified BGK equation and probably finds a unified numerical algorithm for flows over a wide range of Knudsen numbers.

In the 1990s, applying the asymptotic expansion of the molecular velocity distribution function to the Maxwellian distribution based on the flux conservation at the cell interface, new BGK type schemes [10–12] adapted to the gas flows of continuum regime have been presented according to the thoughts of the shock capturing difference method. The schemes have successfully simulated some problems, such as one-dimensional shock wave structures and two-dimensional shock wave reflections, inviscid and viscous turbulent flows, etc. In the computation of the rarefied gas flows, the high resolution explicit and implicit finite-difference methods to solve two-dimensional BGK-Boltzmann model equations have been set forth [9, 13–16] based on the introduction of the reduced velocity distribution functions and the application of the discrete ordinate method. The reliability and efficiency of the methods have been demonstrated in applications to both steady and unsteady one- and two-dimensional rarefied gas dynamical problems.

In this study, based on the basic characteristics of molecular movement and collision approaching to equilibrium, the unified simplified velocity distribution function equation adapted to various flow regimes can be described by introducing the colliding relaxation parameters and the local equilibrium distribution function to revise the BGK equation. The reduced velocity distribution functions can be introduced to reduce the dimensions of the kinetic model equation. The discrete velocity ordinate method [17] is applied to the reduced distribution functions in order to replace their continuous dependency on the velocity space, and then the single kinetic model equation will be cast into hyperbolic conservation equations with non-linear source terms in the physical space and time. Drawing on the decoupling technique [18, 19] on molecular movement and collision in the DSMC method, the unsteady time-splitting method is used to split the distribution function equations into the colliding relaxation equation and the convective movement equations. The non-oscillatory, containing no free parameters and dissipative (NND) scheme [20] is extended and applied to solve the convective equations,

the colliding relaxation equation can be numerically simulated by the aid of the second-order Runge–Kutta method. The gas kinetic finite-difference method for directly solving the discrete velocity distribution functions will be established by the way of coupling and iteration. The mathematical model on the gas kinetic boundary conditions will be developed. To improve computational efficiency for various Mach number flows, three types of quadrature rules are applied to the discrete velocity space to evaluate the macroscopic flow parameters at each point in the physical space. As a result, a unified simplified gas kinetic numerical algorithm will be developed for the gas dynamical problems from various flow regimes. The method is tested in this paper for both the one-dimensional shock tube problems and the flows over two-dimensional circular cylinder with various Knudsen numbers.

2. DESCRIPTION OF THE UNIFIED REDUCED VELOCITY DISTRIBUTION FUNCTION EQUATIONS FOR VARIOUS FLOW REGIMES

Based on the collision spacing theory of microscopic molecular dynamics, the BGK collision model equation can be revised by using the basic feature of molecular movement and collision approaching to equilibrium [1, 5, 7, 21]. The local equilibrium distribution function f^N from the Shakov model [4, 9, 13] is taken as the asymptotic expansion in Hermite polynomials with the local Maxwell distribution function f_M as the weighting function. The collision frequency v of the gas molecules can be described [1, 7–9] by introducing molecular colliding relaxation parameters related to various flow regimes and expressed as the function of density, temperature, the freestream mean free path, and the exponent of molecular power law. The v and the appropriate f^N can be integrated with the macroscopic flow parameters, the molecular viscosity transport coefficients, the thermodynamic effect, the molecular power-law models, and the flow states from various flow regimes [22]. Consequently, the unified simplified molecular velocity distribution function equation which qualitatively describes gas flow characteristics from various flow regimes can be presented with the non-dimensional form in the Cartesian co-ordinates [9, 13, 22].

$$\frac{\partial f}{\partial t} + \mathbf{V} \cdot \frac{\partial f}{\partial \mathbf{r}} = v(f^N - f) \tag{1}$$

$$f^N = f_M \cdot [1 + (1 - Pr)\mathbf{c} \cdot \mathbf{q}(2c^2/T - 5)/(5PT/2)] \tag{2}$$

$$f_M = n/(\pi T)^{3/2} \exp[-c^2/T] \tag{3}$$

$$v = 8nT^{1-\chi}/(5\sqrt{\pi}\,Kn), \quad Kn = \lambda_\infty/L \tag{4}$$

where f is the molecular velocity distribution function which depends on space $\mathbf{r}$, molecular velocity $\mathbf{V}$ and time t. Kn is the Knudsen number related to the ratio of the freestream mean free path λ_∞ to the reference length L of the problem. Pr is the Prandtl number with $Pr = \mu C_p/K$ and is equal to $\frac{2}{3}$ for a monatomic gas, C_p is the specific heat at constant pressure, μ and K, respectively, denote the coefficient of gas viscosity and heat conduction. $\mathbf{q}$ and P, respectively, denote the heat flux vector and gas pressure. $\mathbf{c}$ is the thermal (peculiar) velocity of

the molecule, and c represents the magnitude of the $\mathbf{c}$, that is $\mathbf{c}=\mathbf{V}-\mathbf{U}$ and $c^2=c_x^2+c_y^2+c_z^2$, where the $\mathbf{c}$ consists of $c_x=V_x-U$, $c_y=V_y-V$ and $c_z=V_z-W$ along the x-, y- and z-directions with (U,V,W) corresponding to three components of the mean flow velocity $\mathbf{U}$. χ is the temperature exponent of the coefficient of viscosity which is a constant for a given gas ($=1$ for Maxwell molecules, $=0.75$ for air, $=0.5$ for hard sphere molecules), that can also be denoted as $\chi=(\zeta+3)/(2(\zeta-1))$ for the Chapman–Enskog gas of inverse power law, where ζ is the inverse power coefficient related to the power force F and the distance r between centres of molecules, that is $F=\kappa/r^{\zeta}$ with a constant κ. All of the properties have been non-dimensionalized, each dimensionless quantity is referred to its equilibrium values at upstream infinity (n_∞, T_∞), the reference speed c_∞ is $\sqrt{2RT_\infty}$, the reference force is $mn_\infty c_\infty^2/2$, the reference heat flux is $mn_\infty c_\infty^3/2$ and the reference time t_∞ is L/c_∞, the reference distribution function is n_∞/c_∞^3.

The macroscopic flow parameters, such as the number density, flow mean velocity, temperature, pressure, viscous stress tensor and heat flux vector, can be determined [1, 6, 7, 9, 22] by the moments of the distribution function over the molecular velocity space.

$$n(\mathbf{r},t)=\int f\,\mathrm{d}\mathbf{V} \tag{5}$$

$$nU_i(\mathbf{r},t)=\int V_i f\,\mathrm{d}\mathbf{V} \tag{6}$$

$$\frac{3}{2}nT(\mathbf{r},t)=\int c^2 f\,\mathrm{d}\mathbf{V} \tag{7}$$

$$P=nT \tag{8}$$

$$\tau_{ij}(\mathbf{r},t)=2\int c_i c_j f\,\mathrm{d}\mathbf{V}-P\delta_{ij} \tag{9}$$

$$q_i(\mathbf{r},t)=\int c^2 c_i f\,\mathrm{d}\mathbf{V} \tag{10}$$

where δ_{ij} is the Kronecker delta, the subscripts i and j each range from 1 to 3. The values 1, 2 and 3 may be identified with components along the x-, y- and z-axis, respectively.

2.1. *Reduced distribution function equations for one-dimensional gas flows*

The velocity distribution function Equation (1) for one-dimensional gas flows can be written by

$$\frac{\partial f}{\partial t}+V_x\frac{\partial f}{\partial x}=\nu(f^N-f) \tag{11}$$

The molecular velocity distribution function equation in Equation (11) can be integrated with respect to V_y and V_z with weighting factors 1 and $V_y^2+V_z^2$ so that the number of independent variables in the distribution function f can be reduced by integrating out the dependence of f on V_y and V_z. The following two reduced distribution functions are

introduced [23]:

$$g(x,t,V_x)=\int_{-\infty}^{\infty}\int_{-\infty}^{\infty} f(x,t,V_x,V_y,V_z)\,\mathrm{d}V_y\,\mathrm{d}V_z \tag{12}$$

$$h(x,t,V_x)=\int_{-\infty}^{\infty}\int_{-\infty}^{\infty} (V_y^2+V_z^2) f(x,t,V_x,V_y,V_z)\,\mathrm{d}V_y\,\mathrm{d}V_z \tag{13}$$

Integrating out the V_y and V_z dependence over the model Equation (11), the equivalent system can be obtained [22]:

$$\frac{\partial g}{\partial t}+V_x\frac{\partial g}{\partial x}=\nu(G^N-g) \tag{14}$$

$$\frac{\partial h}{\partial t}+V_x\frac{\partial h}{\partial x}=\nu(H^N-h) \tag{15}$$

2.2. Reduced distribution function equations for two-dimensional gas flows

For analysis of gas flows in x and y directions around two-dimensional bodies, it is convenient to introduce the following reduced distribution functions [9, 13, 14] in order to reduce the number of the independent variables in the distribution function f.

$$g(x,y,t,V_x,V_y)=\int_{-\infty}^{\infty} f(x,y,t,V_x,V_y,V_z)\,\mathrm{d}V_z \tag{16}$$

$$h(x,y,t,V_x,V_y)=\int_{-\infty}^{\infty} V_z^2 f(x,y,t,V_x,V_y,V_z)\,\mathrm{d}V_z \tag{17}$$

The single velocity distribution function Equation (1) can be transformed into two partial differential equations [22]:

$$\frac{\partial g}{\partial t}+V_x\frac{\partial g}{\partial x}+V_y\frac{\partial g}{\partial y}=\nu(G^N-g) \tag{18}$$

$$\frac{\partial h}{\partial t}+V_x\frac{\partial h}{\partial x}+V_y\frac{\partial h}{\partial y}=\nu(H^N-h) \tag{19}$$

The macroscopic flow parameters denoted by the reduced distribution functions can be similarly obtained [22] by substituting the above-mentioned reduced distribution functions g and h into Equations (5)–(10).

3. APPLICATION OF THE DISCRETE VELOCITY ORDINATE METHOD

Based on the principle of probability statistics, the molecular velocity distribution function possesses the property of the exponential function $\exp(-c^2)$ [7, 24, 25], the functional dependency of f on the velocity components (V_x, V_y, V_z) belongs to exponential type, and the

probability of the molecular velocities far removed from the mean velocity **U** of the flow is always negligible. Thus, in order to replace the continuous dependency of the molecular velocity distribution function on the velocity space, the discrete ordinate technique [17, 26] can be introduced in the kinetic theory of gases to discretize the finite velocity region removed from **U**. This method, which consists of replacing the integration over the velocity space of the distribution function by an appropriate quadrature, requires the values of the distribution function only at certain discrete velocity ordinate points. The selection of the discrete velocity ordinate points is only based on the moments of the distribution functions over the velocity space. Consequently, the macroscopic flow moments of the distribution function f over velocity space can be evaluated by the same quadrature procedure with f evaluated at only a few discrete velocity points in the vicinity of **U**. The selections of the discrete velocity points and the range of the discrete velocity space in the discrete ordinate method are somewhat determined by the problem dependent.

Applying the discrete velocity ordinate method [9, 14, 15] to Equations (18) and (19) for the velocity components V_x and V_y, the reduced velocity distribution function equations for two-dimensional gas flows can be transformed into $N_1 \times N_2$ hyperbolic conservation equations with non-linear source terms at each of discrete velocity grid points.

$$\frac{\partial \bar{Q}}{\partial t} + \frac{\partial F^x}{\partial x} + \frac{\partial F^y}{\partial y} = \bar{S} \tag{20}$$

with

$$\bar{Q} = \begin{pmatrix} g_{\sigma,\delta} \\ h_{\sigma,\delta} \end{pmatrix}, \qquad F^x = V_{x\sigma}\bar{Q}$$

$$F^y = V_{y\delta}\bar{Q}, \qquad \bar{S} = \begin{pmatrix} \nu(G^N_{\sigma,\delta} - g_{\sigma,\delta}) \\ \nu(H^N_{\sigma,\delta} - h_{\sigma,\delta}) \end{pmatrix}$$

where $g_{\sigma,\delta}$, $h_{\sigma,\delta}$, $G^N_{\sigma,\delta}$ and $H^N_{\sigma,\delta}$, respectively, denote values of g, h, G^N and H^N evaluated at the discrete velocity grid points $V_{x\sigma}$ and $V_{y\delta}$, and the subscripts σ and δ, respectively, represent the discrete velocity grid indexes in the V_x- and V_y-directions. N_1 and N_2 represent the number of discrete quadrature points used in the V_x and V_y directions, respectively.

Once the discrete velocity distribution functions are solved, the macroscopic flow moments at each point of the physical space can be obtained by the appropriate discrete velocity quadrature method.

In terms of the symmetric quality of the exponential function $\exp(-V^2)$ over the interval $[-\infty, \infty]$, the Gauss–Hermite half-range quadrature from References [26, 27] can be extended and applied to evaluate of the infinite integral over all the velocity space of the velocity distribution function. The discrete velocity points and the weights corresponding to the modified Gauss–Hermite quadrature can be obtained using the algorithms described by Huang and Giddens [27] and by Shizgal [26], which can be used to approximate the integrals with the exponential type as follows:

$$\int_0^\infty \mathrm{e}^{-V^2} p(V)\,\mathrm{d}V \approx \sum_{\sigma=1}^{N} W_\sigma\, p(V_\sigma) \tag{21}$$

where V_σ ($\sigma = 1, \ldots, N$) are the positive roots of the Hermite polynomial of degree N, W_σ are the corresponding weights, the subscript σ is the discrete velocity index, and $p(V)$ denotes the function which can be derived from the integrands in Equations (5)–(10). According to Kopal's discussion [28, 29], it is known that for a given number of discrete subdivisions of the interval $(0, +\infty)$, the Gauss–Hermite's choice of the discrete velocity points V_σ and the corresponding weights W_σ yields the optimal discrete approximation to the considered integration in the sense. The Gauss–Hermite's V_σ and W_σ can be tabulated in the table of the Gauss–Hermite quadrature. However, the number of the discrete velocity points is limited in this way, as indicates that farther application of the Gauss–Hermite quadrature method to high speed gas flows may be restricted. The advantage of using the modified Gauss–Hermite quadrature formula [9, 22] is its high accuracy, but for high freestream Mach number flows, the number of discrete velocity grid points needed to cover the appropriate velocity range could become quite large. To simulate hypersonic flows, the composite integration method based on equally spaced three-point Newton–Cotes formulas and the Gauss–Legendre numerical quadrarure rule whose integral nodes are determined by using the roots of the kth Legendre polynomial have been applied to this study [22].

4. NUMERICAL ALGORITHM ON THE VELOCITY DISTRIBUTION FUNCTION EQUATIONS

4.1. Numerical method for one-dimensional gas flows

Recurring to the discrete velocity ordinate method, the reduced velocity distribution function equations Equations (14) and (15) can be transformed into the hyperbolic conservation laws form at each of discrete velocity points ($V_{x\sigma}, \sigma = 1, \ldots\ldots N$) which can be numerically solved by the finite-difference method of computational fluid dynamics. The dominating equations of the discrete velocity distribution functions g_σ and h_σ for one-dimensional gas flows can be written [22, 30] as

$$\frac{\partial U}{\partial t} + \frac{\partial F}{\partial x} = S \tag{22}$$

with

$$U = \begin{pmatrix} g_\sigma \\ h\sigma \end{pmatrix}, \quad F = V_{x\sigma} U, \quad S = \begin{pmatrix} v(G_\sigma^N - g_\sigma) \\ v(H_\sigma^N - h_\sigma) \end{pmatrix}$$

where g_σ, h_σ, G_σ^N and H_σ^N, respectively, correspond to the values of g, h, G^N and H^N at the discrete velocity ordinate points $V_{x\sigma}$, and the subscripts σ represent the discrete velocity grid indexes in the V_x-direction.

To numerically evaluate the convective part of the set of Equations (22), the NND scheme [20] is used, which is semi-discretized non-oscillatory, contains no free parameters, and is dissipative with the distinguished capability of capturing shock and other contact discontinuities. The term $(\partial U/\partial t)$ in Equation (22) can be discretized using the second-order Runge–Kutta method. As a result, the finite-difference second-order scheme can be constructed for solving

the governing Equations (22) at each of discrete velocity ordinate points, as follows:

$$\begin{aligned} \delta_t U^* &= R(U^n) \\ U^* &= U^n + \Delta t \delta_t U^* \\ \delta_t U^{**} &= R(U^*) \\ U^{n+1} &= U^n + \frac{\Delta t}{2}(\delta_t U^* + \delta_t U^{**}) \end{aligned} \tag{23}$$

The operator $R(U^n)$ is set [20] as

$$R(U^n) = -\frac{1}{\Delta x}(H^n_{i+1/2} - H^n_{i-1/2}) + S^n_i$$

with the numerical flux defined by

$$\begin{aligned} H_{i+1/2} &= F^+_{i+1/2L} + F^-_{i+1/2R} \\ F^+_{i+1/2L} &= F^+_i + \frac{1}{2}\ \text{min mod}(\Delta F^+_{i-1/2}, \Delta F^+_{i+1/2}) \\ F^-_{i+1/2R} &= F^-_{i+1} - \frac{1}{2}\ \text{min mod}(\Delta F^-_{i+1/2}, \Delta F^-_{i+3/2}) \\ \Delta F^\pm_{i+1/2} &= F^\pm_{i+1} - F^\pm_i \end{aligned}$$

Here, $F^+ = A^+U$ and $F^- = A^-U$, respectively, denote the positive and negative fluxes of $F = AU$, and $A = \partial F/\partial U$ is the corresponding Jacobian matrix.

The flux limiter min mod operator is defined by

$$\text{min mod}(x, y) = \tfrac{1}{2}[\text{sgn}(x) + \text{sgn}(y)]\,\text{min}(|x|, |y|) \tag{24}$$

The stable condition of the scheme can be written as [22]

$$\Delta t_s = \text{CFL} \Big/ \left(\frac{v}{2} + \frac{3}{2}\frac{|V_{x\sigma}|}{\Delta x}\right)_{\max} \tag{25}$$

where, CFL is the adjusting coefficient of the time step in the scheme, that is set as CFL = 0.95.

Considering the basic feature of the molecular movement and colliding approaching to equilibrium, the time step size (Δt) in the computation should be controlled by coupling the stable condition (Δt_s) of the scheme with the local mean collision time (Δt_c) [18,31]:

$$\Delta t = \min(\Delta t_s, \Delta t_c) \tag{26}$$

Here, $\Delta t_c = 1/v_{\max}$.

4.2. Numerical algorithm for two-dimensional gas flows

To treat arbitrary geometries, the dominating Equations (20) of the discrete distribution functions $g_{\sigma,\delta}$ and $h_{\sigma,\delta}$, for two-dimensional gas flows can be written [22] in general

co-ordinates (ξ, η):

$$\frac{\partial U}{\partial t} + \frac{\partial F}{\partial \xi} + \frac{\partial G}{\partial \eta} = S \tag{27}$$

Here,

$$U = J\bar{Q}, \quad F = \bar{U}U, \quad G = \bar{V}U, \quad S = J\bar{S}$$

Note that $\bar{U}$, $\bar{V}$ are the so-called 'contravariant molecular velocity' defined as $\bar{U} = V_{x\sigma}\xi_x + V_{y\delta}\xi_y, \bar{V} = V_{x\sigma}\eta_x + V_{y\delta}\eta_y$, J is the Jacobian of the general transformation, that is $J = \partial(x, y)/\partial(\xi, \eta)$. The metric Jacobian and the metric terms of the general transformation are, respectively, denoted as

$$J = x_\xi y_\eta - y_\xi x_\eta, \quad \xi_x = \frac{1}{J} y_\eta, \quad \eta_x = -\frac{1}{J} y_\xi, \quad \xi_y = -\frac{1}{J} x_\eta, \quad \eta_y = \frac{1}{J} x_\xi$$

The Jacobian coefficient matrices $A = \partial F/\partial U$ and $B = \partial G/\partial U$ of the transformed equations (27) are diagonal and have real eigenvalues $a = \bar{U}$ and $b = \bar{V}$, and the eigenvalue of $\partial S/\partial U$ is taken as $c = -v$.

Based on the Taylor expanding with the second-order accuracy in time, the time-splitting method for the unsteady equation can be extended and employed to decompose Equation (27) into the colliding relaxation equation with the non-linear source terms and the convective movement equations in position space so as to couple to solve them in the computation [22, 30].

$$\begin{aligned} U^{n+1} &= U^n - \Delta t(1 + c\Delta t)(a\delta_\xi + b\delta_\eta)U^n + \frac{\Delta t^2}{2}(a^2\delta_{\xi^2} + 2ab\delta_{\xi\eta} + b^2\delta_{\eta^2})U^n \\ &\quad + \Delta t\left(1 + \frac{c}{2}\Delta t\right)S^n + O(\Delta t^2, \Delta\xi^2, \Delta\eta^2) \\ &= \left[1 - a\Delta t\delta_\xi + \frac{a^2}{2}\Delta t^2\delta_{\xi^2}\right]\left[1 - b\Delta t\delta_\eta + \frac{b^2}{2}\Delta t^2\delta_{\eta^2}\right] \\ &\quad \times \left[1 + c\Delta t\left(1 + \frac{c}{2}\Delta t\right)\right]U^n + O(\Delta t^2, \Delta\xi^2, \Delta\eta^2) \end{aligned}$$

The above-mentioned difference scheme can be split as

$$U^* = L_s(\Delta t)U^n = U^n + \left(1 - \frac{v}{2}\Delta t\right)\Delta t S^n \tag{28}$$

$$U^{**} = L_\eta(\Delta t)U^* = \left[1 - b\Delta t\delta_\eta + \frac{b^2\Delta t^2}{2}\delta_{\eta^2}\right]U^* \tag{29}$$

$$U^{n+1} = L_\xi(\Delta t)U^{**} = \left[1 - a\Delta t\delta_\xi + \frac{a^2\Delta t^2}{2}\delta_{\xi^2}\right]U^{**} \tag{30}$$

It can be shown that the difference expressions of Equations (28), (29) and (30) are, respectively, in accord with differential equations

$$\frac{\partial U}{\partial t} = S \tag{31}$$

$$\frac{\partial U}{\partial t} + \frac{\partial G}{\partial \eta} = 0 \tag{32}$$

$$\frac{\partial U}{\partial t} + \frac{\partial F}{\partial \xi} = 0 \tag{33}$$

For the first step in the computation, the equation $\partial U/\partial t = S$ with non-linear source item can be solved by the improved Euler method.

$$\begin{aligned} \delta_t U^* &= \left(1 - \frac{v}{2}\Delta t\right) S(U^n) \\ U^* &= U^n + \Delta t \delta_t U^* \\ \delta_t U^{**} &= \left(1 - \frac{v}{2}\Delta t\right) S(U^*) \\ U^{n+1} &= U^n + \frac{\Delta t}{2}(\delta_t U^* + \delta_t U^{**}) \end{aligned} \tag{34}$$

For the second step, the convective movement equation $\partial U/\partial t + \partial G/\partial \eta = 0$ can be numerically solved by the NND-4(a) scheme [32] which is two-stage predictor–corrector scheme with second-order accuracy in time and space.

$$U^* = U^n - \frac{\Delta t}{\Delta \eta}(H^n_{j+1/2} - H^n_{j-1/2}) \tag{35}$$

$$U^{n+1} = \frac{1}{2}\left[U^n + U^* - \frac{\Delta t}{\Delta \eta}(H^*_{j+1/2} - H^*_{j-1/2})\right] \tag{36}$$

$$H_{j+1/2} = G^+_{j+1/2,L} + G^-_{j+1/2,R}$$

$$G^+_{j+1/2,L} = G^+_j + \frac{1}{2}\ \text{min mod}(\Delta G^+_{j-1/2}, \Delta G^+_{j+1/2})$$

$$G^-_{j+1/2,R} = G^-_{j+1} - \frac{1}{2}\ \text{min mod}(\Delta G^-_{j+1/2}, \Delta G^-_{j+3/2})$$

For the third step, the equation $\partial U/\partial t + \partial F/\partial \xi = 0$ is equally solved by the NND-4(a) scheme.

Considering simultaneously proceeding on the molecular movement and colliding relaxation in real gas, the computing order of the previous and hind time steps is interchanged to couple to solve the convective parts and the source term in the computation. The finite-difference

second-order scheme directly to solve the discrete velocity distribution functions is developed as

$$U^{n+1} = L_s(\Delta t/2)L_\eta(\Delta t/2)L_\xi(\Delta t)L_\eta(\Delta t/2)L_s(\Delta t/2)U^n \tag{37}$$

In the aforementioned scheme, the integration operator $L_s(\Delta t)$ of the source term is done using the improved Euler method defined by Equation (34). The one-dimensional space operator $L_\eta(\Delta t)$ and $L_\xi(\Delta t)$ of the convective movement are respectively approximated by the NND-4(a) scheme defined by Equations (35) and (36). The time step Δt in the computation [22, 30, 31] can be determined by the following stability conditions:

$$\Delta t = \min(\Delta t_c, \Delta t_s) \tag{38}$$

Here, $\Delta t_s = \mathrm{CFL}/\max(v/2, |\bar{U}|/\Delta\xi, |\bar{V}|/\Delta\eta)$.

4.3. Numerical implementation of boundary conditions

In the kinetic theory of gases, the interaction between the gas and the body surface is expressed by the boundary condition acting on the molecular velocity distribution function. The distribution function of the gas molecules near the surface will not be an equilibrium distribution. At the present, the models describing the interaction of the gas with the solid surface are largely phenomenological in nature [7], the most widely used models have specular reflection, perfect diffuse reflection, and the combination of both. The perfect diffuse reflection is applied in this study [22]. In order to specify the interaction of the molecules with the solid surface, it is assumed that molecules which strike the surface are subsequently emitted with a Maxwellian velocity distribution fully accommodating to the wall temperature T_w and velocity (U_w, V_w).

For $\mathbf{c}\cdot\mathbf{n} > 0$ in the wall cells of two-dimensional flows [9, 13, 22]

$$g_{w\sigma,\delta} = \frac{n_w}{\pi T_w}\exp\left(-\frac{(V_{x\sigma}-U_w)^2+(V_{y\delta}-V_w)^2}{T_w}\right) \tag{39}$$

$$h_{w\sigma,\delta} = T_w g_{w\sigma,\delta}/2 \tag{40}$$

Here, the density of molecules diffusing from the surface, n_w, which is not known previously, must be determined by means of a further condition. For an impermeable wall, the particle fluxes normal to the wall vanish from the mass balance condition on the surface. That is

$$\int_{c_n>0} c_n f \,\mathrm{d}\mathbf{V} = \int_{c_n<0} -c_n f \,\mathrm{d}\mathbf{V} \tag{41}$$

$$n_w = -2\left(\frac{\pi}{T_w}\right)^{1/2}\int_{-\infty}^{\infty}\int_{-\infty}^{\infty} c_n^- g(x, y, t, V_x, V_y)\,\mathrm{d}V_x\,\mathrm{d}V_y \tag{42}$$

where, $c_n = (V_x - U)n_x + (V_y - V)n_y$, $c_n^- = (c_n - |c_n|)/2$, and $\mathbf{n}$ is the outward unit vector normal to the solid surface.

For $\mathbf{c}\cdot\mathbf{n} \leqslant 0$, the discrete velocity distribution functions at the wall cells are solved by using second-order upwind-difference approximations from the adjacent grids.

The distribution function is assumed to be in equilibrium at infinity. However, the outer boundary must be in some finite distance from the body, so the outer boundary conditions are treated using characteristics-based boundary conditions which are in accord with the upwind nature of the interior point scheme [13, 22]. From this standpoint, the reduced distribution functions for outgoing molecules through the outer boundaries are determined by the second-order difference approximation from the interior points. For molecules incoming from outside, the following conditions are used for the calculation to the boundary cells: (1) Along upstream boundary ahead of the body, the distribution functions of the ingoing molecules from upstream are set as an equilibrium distribution with prescribed free stream properties. (2) In the downstream boundary, it is assumed that there is no gradient along the outward direction for the distribution function; that is, for incoming molecules:

$$\frac{\partial \Delta U}{\partial \eta} = 0 \tag{43}$$

For flow problems with symmetry, the half-flow field is only computed by the way where the symmetric boundary is displaced outwards from the symmetric line of the flow field to increase fictitious cells so that the cells along the symmetric line are processed as interior points and the symmetry conditions are assigned to the distribution functions along the symmetrical line of the flow field [22]. The molecular velocity distribution functions f^r in the fictitious cells can be expressed by the distribution functions of the interior flow field:

$$f^r(\mathbf{r}, \mathbf{V}, t) = f(\mathbf{r} - 2(\mathbf{n} \cdot \mathbf{r})\mathbf{n}, \mathbf{V} - 2(\mathbf{n} \cdot \mathbf{V})\mathbf{n}, t) \tag{44}$$

where $\mathbf{n}$ is the unit vector normal to the symmetrical line and pointing to the interior of the flow field.

5. NUMERICAL EXAMPLES AND RESULTS

The one-dimensional shock-tube problems and the flows past two-dimensional circular cylinder with various Knudsen numbers are computed to illustrate the accuracy of the present numerical method and to demonstrate its reliability in solving the gas dynamical problems from rarefied flow to continuum. In the computation, the convergence of a steady-state solution is assumed to have occurred when the quadratic global relative error of the flow quantities (e.g. density, flow velocity, temperature), which are evaluated by the discrete velocity numerical integration methods described in Section 3, between successive iteration steps is less than 10^{-4}.

5.1. One-dimensional shock-tube problems with various Knudsen numbers

5.1.1. Unsteady Riemann shock-tube problem. This problem can be described by the way where a diaphragm located at $x = 0.5$ divides a one-dimensional flow field into two regions, each in a constant equilibrium state at $t = 0$. Here the case is considered with initial states: $\rho = 0.445,\ T = 13.21,\ u = 0.698$ for $0.0 \leqslant x \leqslant 0.5$ and $\rho = 0.5, T = 1.9, u = 0.0$ for $0.5 < x \leqslant 1$. The ratio of specific heats γ is $\frac{5}{3}$ for a monatomic Maxwell gas. The cell size $\Delta x = 0.01$ in the physical space was set and the 6-points Gauss–Legendre numerical quadrature rule with the discrete velocity sub-spacing $\Delta V = 2.0$ was employed to evaluate the macroscopic

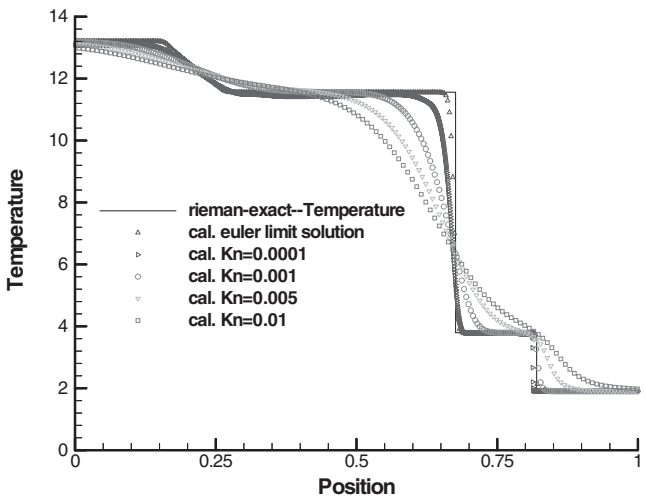

Figure 1. Temperature profiles of shock-tube problem for various Kn.

flow moments over the velocity space, which has 61 discrete velocity grid points ranging from -10 to 10. The computing time step (Δt) was determined by Equation (26). The computational results (denoted as symbols) of non-dimensional temperature profiles for $Kn = 0.01, 0.005, 0.001, 0.0001$ at time $t = 0.1314$ are presented in Figure 1. To see the contribution of the collision relaxation term in the gas kinetic model equation to the distribution function, we test a numerical method which is generated from Equation (1) by neglecting the collision source term and setting the distribution function in convective term equal to the equilibrium Maxwellian distribution ($f = f_{\mathrm{M}}$). The solution obtained by such a scheme is named as the Euler limit solution of continuum flow. It is shown from Figure 1 that the bigger is the Knudsen number, the thicker is the shock wave. The smaller is the Knudsen number down to $Kn = 0.0001$, the crisper shock and expanding wave profiles are given. The results appropriate to $Kn = 0.0001$ are in good agreement with the computed Euler limit solution and the Riemann exact solution. Figure 1 qualitatively reveals the changing process that the gas flow becomes from rarefied flow to continuum along with diminishing the Knudsen number.

5.1.2. The normal shock-structure problem. In the case of the normal shock wave, a shock wave involves the transition from a uniform supersonic upstream (state 1) to a uniform subsonic downstream (state 2). The shock Mach number M_{s} is defined as the ratio of the speed of the wave, relative to the upstream gas, to the speed of sound in this gas. The upstream state is chosen as the reference state with $\rho_1 = 1,\ T_1 = 1$ and $P_1 = 1$. The relations of the flow states (upstream ρ_1, T_1, U_1 and downstream ρ_2, T_2, U_2) across the wave are defined in terms of the Rankine–Hugoniot conditions. The flow region is extended over a distance $-x_1 < x < x_2$. A discontinuity between upstream and downstream states was set at $x = 0$ as the initial condition. The case of $M_{\mathrm{s}} = 8$ for argon gas is computed with $Pr = 2/3,\ \gamma = 5/3$. The space grid points used are 121 with $\Delta x = 0.25\lambda_1$, and the Newton–Cotes quadrature formula was employed to evaluate the macroscopic flow moments with 121 discrete velocity ordinate points using the discrete velocity spacing $\Delta V = 0.35$. The length scale is normalized by the mean

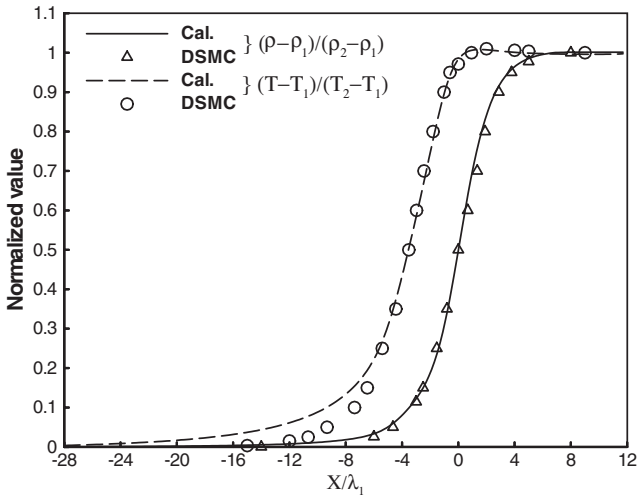

Figure 2. Comparison of computed temperature and density profiles with DSMC results for $M_s = 8$.

free path (λ_1) in front of the shock wave. The quoted mean free path is defined in terms of the coefficient of viscosity by Equation (4.52) from Reference [6]. The molecular model parameters for argon are employed from Appendix A in Reference [6]. The coefficient of gas viscosity has been assumed as the power-law temperature dependence, that is $\mu \propto T^{\chi}$. Here, the viscosity index is set as $\chi = 0.75$. In Figure 2, the computed results for the density and temperature profiles are compared with Bird's DSMC results from Reference [6], where the line denotes the computed results and the symbols denote the DSMC results. The density is normalized in terms of the densities ρ_1 and ρ_2 in front of and behind the shock wave as indicated in the figure. The normalized values of the temperature are defined in a similar manner. The origin has been set at the point in the profile when the density is midway between the upstream and downstream values. It is shown from Figure 2 that the overall agreement is good and the agreement of density is better than that of temperature between the DSMC results and the present calculation.

The viscous shear stress and heat flux vector are sensitive quantities inside the shock, which are defined by Equations (9) and (10). Figures 3 and 4, respectively, show the computed results for the heat flux and viscous shear stress profiles in the x-direction for the above case of $M_s = 8$, along with the comparison with the DSMC results from Reference [33], where the heat flux q_x has been normalized by dividing by the product of the density and the cube of the most probable velocity in the undisturbed gas, and the viscous shear stress τ_{xx} has been normalized by dividing by the product of the density and the square of the most probable velocity in the undisturbed gas. The origin has been set at the point in the profile where the density is midway. It can be shown from Figures 3 and 4, for the high Mach number ($M_s = 8$) shock flow, the profiles of the viscous stress and heat flux exist high deviation from the symmetric equilibrium distribution and appear the prominent asymmetric distribution based on the centre of the wave, and the qualitative agreement between the DSMC results and the present calculation can be obtained, however, the difference increases in the front of the shock wave.

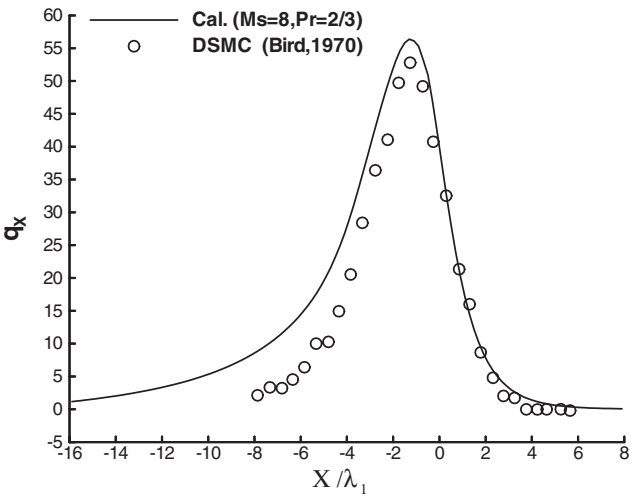

Figure 3. Heat flux profiles in the interior of the shock wave for $M_s = 8$.

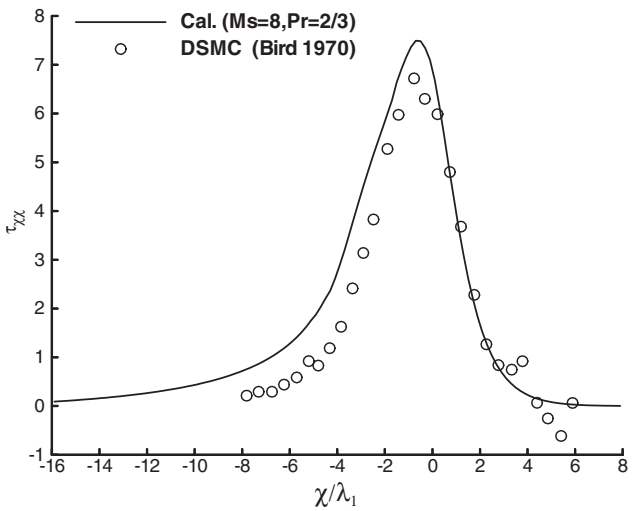

Figure 4. Viscous stress profiles in the interior of the shock wave for $M_s = 8$.

5.2. *Supersonic flows past circular cylinder*

The steady supersonic flows past a circular cylinder under different freestream Mach (M_∞) and Knudsen numbers are computed. Here, due to symmetry, only half-plane on the cylinder is considered and symmetry boundary conditions were employed. The mesh system used is 71×51 (streamwise $\times$ surface normal) in the physical space and the modified Gauss–Hermite quadrature formula with 32×16 discrete velocity ordinate points in the V_x- and V_y-direction was employed. In Figure 5, the comparisons between the calculated cylinder drag coefficients and experimental data for argon gas are given for the cases of $M_\infty = 1.96$, the ratio of the wall

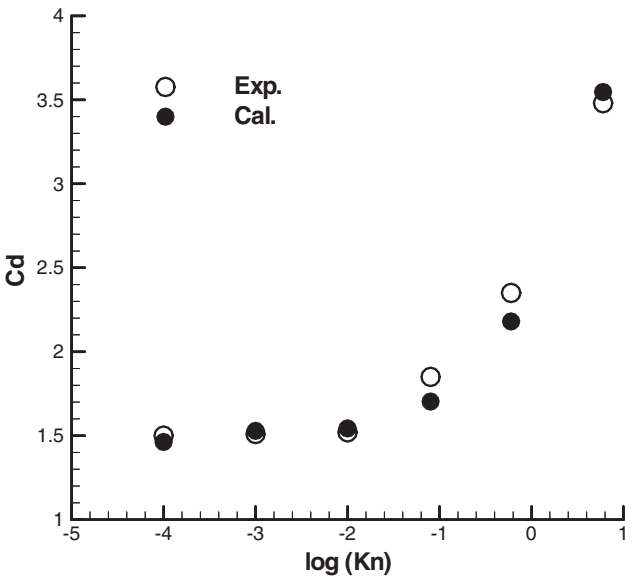

Figure 5. Drag coefficients of the circular cylinder with various *Kn*.

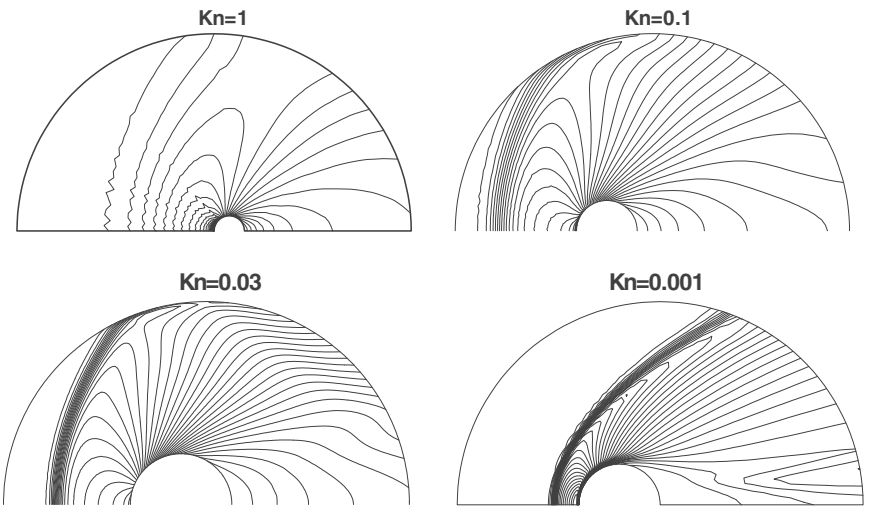

Figure 6. Density contours of the cylinder for the supersonic flow with various *Kn*.

temperature to the total temperature $T_w/T_0 = 0.7$, $Pr = 2/3$, $\gamma = 5/3$, $Kn = 6$, 0.6, 0.08, 0.01, 0.001 and 0.0001. The symbols (○) denote the experimental data from Reference [34] and the relevant continuum flow limit solution, the symbols (●) denote the computed results. It is shown that the computed results agree with the experimental data well. The computed results of the density contours past the circular cylinder with various Knudsen numbers are shown in Figure 6, in respect of the flow states of $Pr = 1, T_w/T_0 = 1$, $\gamma = 5/3$, $M_\infty = 1.8$, $Kn = 1$,

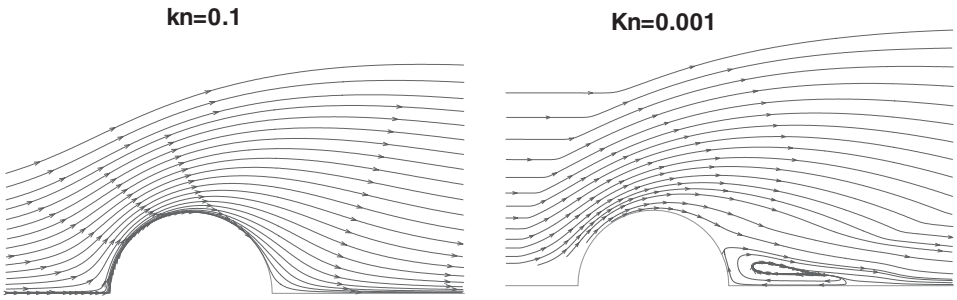

Figure 7. Streamline structure past circular cylinder with various Kn.

0.1, 0.03 and $M_\infty = 4$, $Kn = 0.001$. Figure 7 shows the enlarged views of the streamline past the circular cylinder for the cases of $Kn = 0.1$ and $Kn = 0.001$. It is shown in Figures 6 and 7 that there is no obvious shock wave disturbing region for the fully rarefied flow related to $Kn = 1$, for the near continuum flow of $Kn = 0.001$, the flow structures including the front bow shock, stagnation region and near wake are well captured, and the thickening of the front bow shock are the noticeable differences in the more rarefied cases of $Kn = 0.1$, 0.03. The smaller is the Knudsen number, the thinner and clearer is the bow shock occurring in front of the body. Figures 6 and 7 qualitatively reveal that the gas flow approaches to continuum flow from rarefied transitional flow while the Knudsen number is diminishing from $Kn = 1$ to 0.001. To qualitatively test the reliability of the computed results of the macroscopic flow parameters in the flow field, Figure 8(a) and 8(b) show the comparison between the present computed results for the density, pressure and Mach number contours past the cylinder and Yang and Huang's calculation from Reference [9] for the above case of $Kn = 0.1$, $M_\infty = 1.8$. It can be shown that good agreement of the two results is obtained from Figure 8.

To try out the computation of the present algorithm for the two-dimensional continuum gas flow past the circular cylinder, the case of $Kn = 0.0001$, $M_\infty = 1.8$, $Pr = 2/3$, $T_w/T_0 = 1$ and $\gamma = 5/3$ was set with the 71×51 space cells and the modified Gauss–Hermite quadrature formula with 32×16 discrete velocity grid points. The computed results of Mach number contours are shown in Figure 9. The flow structures including the front bow shock, the stagnation region, the recompression shock, and the wake region are captured very well. Figure 10 shows an enlarged view of the streamlines past the circular cylinder, as is just so the feature of the continuum flow.

The stagnation line profiles of flow velocity are shown in Figure 11 together with the DSMC results [35] for two Knudsen numbers ($Kn = 1, 0.3$) with the flow states of $M_\infty = 1.8$, $Pr = 1$, $T_w/T_0 = 1$ and $\gamma = 1.4$. Here, the space grid system used is 41×35, and the modified Gauss–Hermite quadrature formula with 32×16 discrete velocity ordinate points was employed. In Figure 11, the quantities (U/U00) in the vertical axes denote the non-dimensional velocity values (U/U_∞), and the quantities (X/LMD00) in the horizontal axes denote the non-dimensional distance (X/λ_∞) far from the stagnation point. In general, good agreement between the present computations and DSMC solutions can be observed. However, it's shown from Figure 11 that, as X/λ_∞ in the horizontal axis approaches to the stagnation point, the decreasing rate of the flow velocity U/U_∞ in the present computations is smaller than that in the DSMC results for the case of $Kn = 0.3$. With regard to the reasons, it's may be likely to

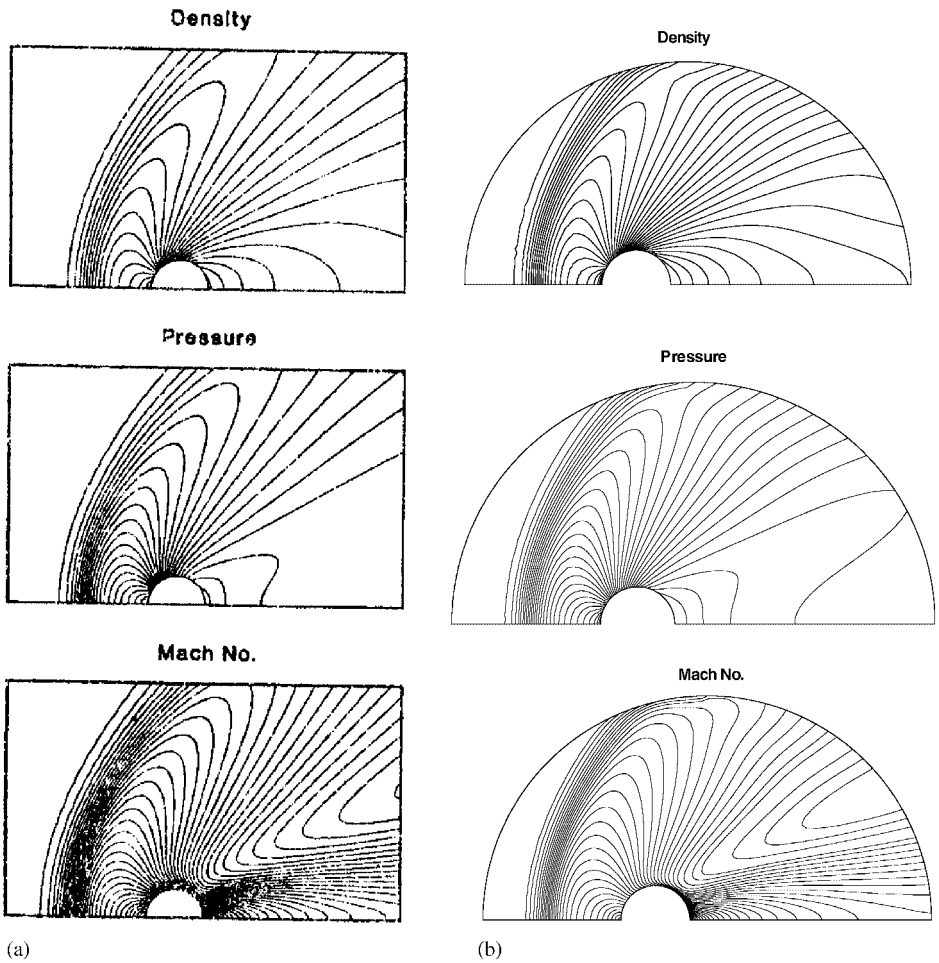

Figure 8. Density, pressure and Mach number contours past the cylinder for $Kn = 0.1$, $M_\infty = 1.8$, (a) Yang and Huang's results from Reference [9]; (b) the present computed results.

use excessively coarse mesh system (41×35) in the computation. For the rarefied transition flow of the case of $Kn = 0.3$, there exists the thicker shock disturbing region in front of the circular cylinder so that the flow velocity drops more slowly and exists discontinuous decline, as need more refined grids to catch the shock disturbing region. On the other hand, the DSMC method provides certain statistical fluctuation with the simulated results, as also affects the comparison.

6. CONCLUDING REMARKS

In this work, the non-linear Boltzmann model equation is transformed into the hyperbolic conservation equations with non-linear source terms by introducing the reduced velocity dis-

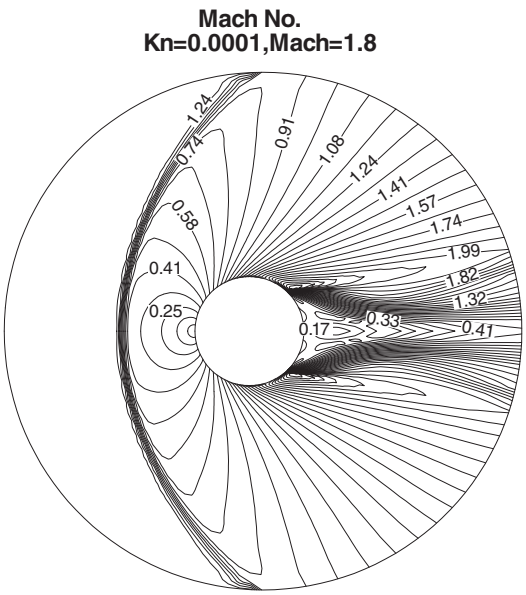

Figure 9. Mach number contours past the cylinder for $Kn = 0.0001$, $M_\infty = 1.8$.

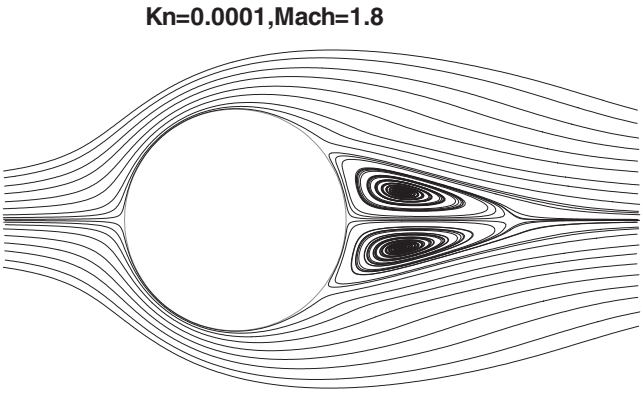

Figure 10. Enlarged view of streamlines past the cylinder with $Kn = 0.0001$.

tribution functions and applying the discrete velocity ordinate method. Based on the Taylor expanding with second-order accuracy, the time-splitting method for the unsteady equation and the uncoupling technique on molecular movement and colliding from DSMC method are used to split up the velocity distribution function equation into the colliding relaxation equation and the convective movement equations. The NND finite-difference scheme is employed to solve convective equations and the second-order Runge–Kutta method is used to numerically simulate the colliding relaxation equation. The mathematical models for the gas–surface

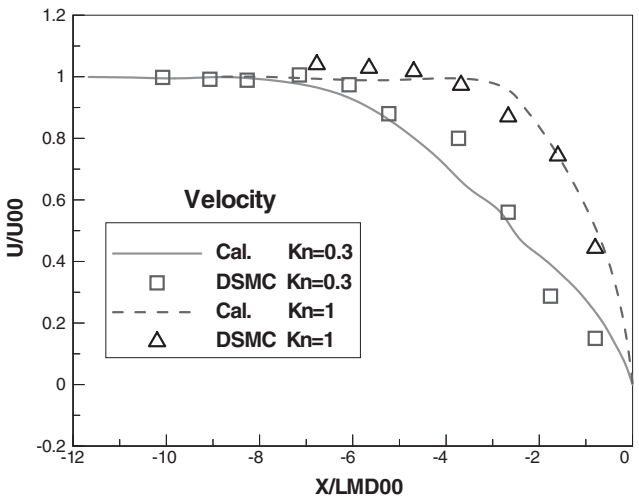

Figure 11. Stagnation line velocity profiles for a circular cylinder.

interactions and gas kinetic boundary conditions are studied and used in the numerical method. As a result, a unified simplified gas kinetic algorithm for the gas dynamical problems from various flow regimes has been developed. The computations of one- and two-dimensional gas flows from rarefied transition to continuum indicate that both high resolution of flow fields and good qualitative agreement with theoretical, DSMC and experimental results can be obtained. The present method provides an economical and efficient way that the velocity distribution function equation describing microscopic molecular transport phenomena can be transformed into hyperbolic conservation equations to be numerically solved with the finite-difference method of computational fluid dynamics and that the gas dynamical problems from rarefied flow to continuum can be effectively simulated. The present method has been extending and applying to simulate three-dimensional gas flows. In addition, farther investigation on the choice and reduction of the number of discrete velocity ordinate points in velocity space to simulate high Mach number flows will be processed, and the present numerical method itself need to be further studied.

It has been shown from the above computations that the results of the present method are not sensitive to the grid spacing in the physical space or the velocity space if only the computing precision be satisfied; however, the finer is the grid, the better should be the precision of the results for certain at the expense of more computing memory and time. The present method is considerable stable and efficient without the limitation of the cell size, unlike the DSMC method which exists statistical fluctuations and requires the grid spacing have to be less than the mean free path. In general, the computational speed for the present method seems be faster than the DSMC method in computing one- and two-dimensional problems of the rarefied flows. As the molecular mean collision time in the continuum flow regime is little, the computing time step given by Equation (38) will be quite little at the magnitude of 10^{-5}, therefore, the convergent speed of the present method seems be slower than that of the Navier–Stokes solver for continuum flows with the Knudsen number subjacent to 10^{-4}.

It has been shown from the computations that the CPU runtime required for the present method increases as the Knudsen number decreases from rarefied flow regime to continuum flow regime, and the computations of the one- and two-dimensional flows can be processed in the 128M or so microcomputers.

ACKNOWLEDGEMENTS

The authors thank Prof. J.Y. Yang and Prof. K. Xu for their helpful discussion. Special thanks are due to the referees and editor for their many valuable comments. The work was supported by the National Nature Science Foundation of China under Grant Nos. 19972008 and 10072077, the Hypervelocity Aerodynamics Institute of CARDC in Mianyang, and the National Laboratory on Computation Fluid Dynamics in Beijing.

REFERENCES

1. Chapmann S, Cowling TG. *The Mathematical Theory of Non-Uniform Gases* (3rd edn). Cambridge University Press: Cambridge, MA, 1990.
2. Bhatnagar PL, Gross EP, Krook M. A model collision processes in gases. I. Small amplitude processes is charged and neutral one-component system. *Physical Review* 1954; **94**:511–525.
3. Holway JR LH. New statistical models for kinetic theory, methods of construction. *Physics of Fluids* 1966; **9**:1658–1673.
4. Shakov EM. Kinetic model equations and numerical results. In *Proceedings of 14th International Symposium on Rarefied Gas Dynamics*, Vol. 1, Oguchi H (eds.). University of Tokyo Press: Tokyo, 1984; 137–148.
5. Ying CT. *The Gas Transport Theory and Application*. Tsinghua University Press: Beijing, China, 1990 (in Chinese).
6. Bird GA. *Molecular Gas Dynamics and the Direct Simulation of Gas Flows*. Clarendon Press: Oxford, 1994.
7. Park DC. *The Kinetic Theory of Gases with Applications in Rarefied Gas Dynamics*. University of Strathclyde: Glasgow, Scotland, 1981.
8. Cercignani C. *Rarefied Gas Dynamics*: *From Basic Concepts to Actual Calculations*. Cambridge University Press: Cambridge, MA, 2000.
9. Yang JY, Huang JC. Rarefied flow computations using nonlinear model Boltzmann equtions. *Journal of Computational Physics* 1995; **120**:323–339.
10. Prendergast KH, Xu K. Numerical hydrodynamics from gas-kinetic theory. *Journal of Computational Physics* 1993; **109**:53–66.
11. Xu K. Gas-kinetic schemes for unsteady compressible flow simulations. Von Karman Institute for Fluid Dynamics Lecture Series. *Proceedings of the 29th Computational Fluid Dynamics*, 1998.
12. Chae D, Kim C, Rho OH. Development of an improved gas-kinetic BGK scheme for inviscid and viscous Flows. *Journal of Computational Physics* 2000; **158**:1–27.
13. Morinishi K, Oguchi H. A computational method and its application to analyses of rarefied gas flows. In *Proceedings of 14th International Symposium on Rarefied Gas Dynamics*, Vol. 1, Oguchi H (ed.). University of Tokyo Press: Tokyo, 1984; 149–158.
14. Bergers D. Kinetic model solution for axisymmetric flow by the method of discrete ordinates. *Journal of Computational Physics* 1985; **57**:285–302.
15. Deng ZT, Liaw GS, Chou LC. Numerical investigation of low-density nozzle flow by solving the Boltzmann model equation. NASA-TM-110492. In *Proceedings of 33rd Aerospace Science Meeting and Exhibit*, 9–12 January, 1995.
16. Aoki K, Kanba K, Takata S. Numerical analysis of a supersonic rarefied gas flow past a flat plate. *Physics of Fluids* 1997; **9**(4):1144–1161.
17. Huang AB, Giddens DP. The discrete ordinate method for the linearized boundary value problems in kinetic theory of gases. In *Proceedings of 5th International Symposium on Rarefied Gas Dynamics*, Brundin CL (ed.). Academic Press: New York, 1967; 481–486.
18. Bird GA. *Molecular Gas Dynamics*. Claredon Press: Oxford, 1976.
19. Shen C. DSMC method and development on the computational of rarefied gas flows. *Advances in Mechanics* 1996; **26**(1):1–12 (in Chinese).
20. Zhang HX. Non-oscillatory and non-free-parameter dissipation difference scheme. *Acta Aerodynamica Sinica* 1988; **6**(2):143–165 (in Chinese).
21. Huang ZQ, Ting EJ. *Transport Theory*. Science Press: Beijing, China, 1987 (in Chinese).

22. Li ZH. Study on the unified algorithm from rarefied flow to continuum. *Ph.D. Dissertation*, China Aerodynamics Research and Development Centre, Mianyang, China, 2001 (in Chinese).
23. Chu CK. Kinetic-theoretic description of the formation of a shock wave. *Physics of Fluids* 1965; **8**(1):12–22.
24. Riedi PC. *Thermal Physics*: *An Introduction to Thermodynamics*, *Statistical Mechanics and Kinetic Theory*. The Macmillan Press Ltd.: London, 1976.
25. Brittin WE. *Lectures in Theoretical Physics*: *Kinetic Theory*, Vol. IX C. Gordon and Breach Science publishers: New York, London, Paris, 1967.
26. Shizgal B. A Gaussian quadrature procedure for use in the solution of the Boltzmann equation and related problems. *Journal of Computational Physics* 1981; **41**:309–327.
27. Huang AB, Giddens DP. A new table for a modified (half-range) Gauss–Hermite quadrature with an evaluation of the integral. *Journal of Mathematical Physics* 1968; **47**:213–218.
28. Kopal Z. *Numerical Analysis*. Chapman & Hall Ltd.: London, 1955.
29. Yan QJ. *Numerical Analysis* (Beijing University of Aeronautics and Astronautics). BUAA Press: Beijing, China, 1994 (in Chinese).
30. Li ZH, Zhang HX. Preliminary study of gas kinetic unified algorithm from rarefied flow to continuum. *Acta Aerodynamica Sinica* 2000; **18**(3):255–263 (in Chinese).
31. Li ZH. DSMC Simulation of hypersonic flow past spacecraft. In *Proceedings of ASIA Workshop on Computational Fluid Dynamics*, Zhang FG (ed.). Sichuan: China, 1994; 97–100.
32. Zhang HX, Zhuang FG. NND Schemes and their application to numerical simulation of two- and three-dimensional flows. *Advances in Applied Mechanics* 1992; **29**:193–256.
33. Bird GA. Aspects of the structure of strong shock waves. *Physics Fluids* 1970; **13**(5):1172–1177.
34. Maslach GJ, Schaaf SA. Cylinder drag in the transition from continuum to free-molecule flow. *Physics of Fluids* 1963; **6**(3):315–321.
35. Vogenitz FW, Bird GA, Broadwell JE. Theoretical and experimental study of rarefied supersonic flows about several simple shapes. *AIAA Journal* 1968; **6**(12):2388–2394.

